CHAPTER TEN

Mathematical Modeling of Regenerative Processes

Osvaldo Chara*, Elly M. Tanaka†, Lutz Brusch*,1
*Center for Information Services and High Performance Computing (ZIH), Technische Universität Dresden, Dresden, Germany
†Center for Regenerative Therapies Dresden (CRTD), Dresden, Germany
1Corresponding author: e-mail address: lutz.brusch@tu-dresden.de

Contents

Abstract

In many animals, regenerative processes can replace lost body parts. Organ and tissue regeneration consequently also hold great medical promise. The regulation of regenerative processes is achieved through concerted actions of multiple organizational levels of the organism, from diffusing molecules and cellular gene expression patterns up to tissue mechanics. Our intuition is usually not adapted well to this degree of complexity and the quantitative aspects of the regulation of regenerative processes remain poorly understood. One way out of this dilemma lies in the combination of

Current Topics in Developmental Biology, Volume 108
ISSN 0070-2153
http://dx.doi.org/10.1016/B978-0-12-391498-9.00011-5

experimentation and mathematical modeling within an iterative process of model development/refinement, model predictions for novel experimental conditions, quantitative experiments testing these predictions, and subsequent model refinement. This interdisciplinary approach has already provided key insights into smaller scale processes during embryonic development and a so-far limited number of more complex regeneration processes. This review discusses selected theoretical and interdisciplinary studies and is structured along the three phases of regeneration: (1) initiation of a regeneration response, (2) tissue patterning during regenerate growth, (3) arresting the regeneration response. Moreover, we highlight the opportunities provided by extensions of mathematical models from developmental processes toward the study of related regenerative processes.

1. INTRODUCTION

The regeneration of lost body parts is a spectacular biological phenomenon (Goss, 1969; Stocum, 2012; for recent reviews, see Birnbaum & Sánchez Alvarado, 2008; Tanaka & Reddien, 2011). In general, the tissue remaining after amputation or autotomy induces one of two alternative responses: scar formation versus regeneration (Fig. 10.1A). Scar formation on the wound site prevents the regenerative response but is not at all understood in evolutionary terms (Bely & Nyberg, 2009). We can speculate that scar formation is a compromise solution that the evolution of complex organisms had to face, in analogy to a frustrated system (Binder, 2008). Most tissues in higher organisms follow this fate of scar formation when damaged.

On the regeneration-competent side, the fresh water polyp *Hydra* initiates a successful and robust regenerative response after head amputation (Browne, 1909; Galliot, 2012; Trembley, 1744) and even from small cell aggregates (Gierer et al., 1972). The more complex planaria (e.g., *Schmidtea mediterranea*) regenerate the entire body plan from almost any tiny body fragment (Gurley, Rink, & Sánchez Alvarado, 2008; Morgan, 1904). A regenerative response can also be found in some vertebrates (Brockes & Kumar, 2005; Murawala, Tanaka, & Currie, 2012; Tanaka, 2003). The zebrafish (*Danio rerio*) regenerates the fin and parts of the eye, heart, and brain (Poss, 2010). The salamander *Amblystoma mexicanum*, as its most spectacular feat, regenerates the entire limb after upper-limb amputation (Goss, 1969; Nacu & Tanaka, 2011). More complex organisms like mammals still regenerate blood, bone, skin, and liver. Organ and tissue regeneration consequently also hold great medical promise. However, the understanding of design principles

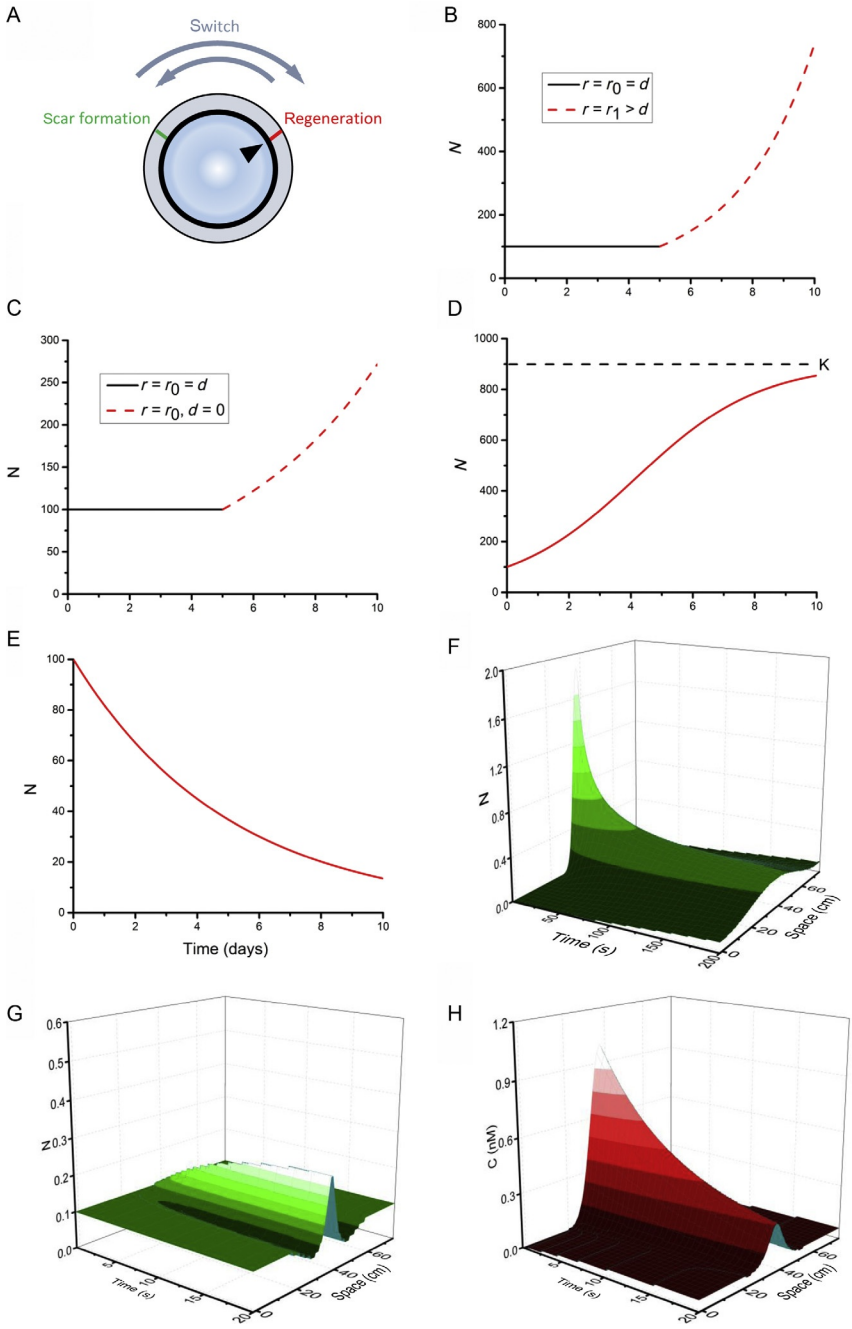

Figure 10.1 *Mathematical models of cell proliferation, apoptosis, and cell migration*. (A) A hypothetical switch illustrating that after amputation, some tissues regenerate whereas others in the same organism, or at an older age or in a closely related species, (*Continued*)

remains poorly understood even in the regeneration-competent model organisms. Such understanding is an absolute prerequisite for future medical applications.

Regenerative processes occur broadly throughout the animal kingdom but even closely related species like different planarian species possess very different regenerative capacities and many lower organisms are not capable of a robust regenerative response (Bely & Nyberg, 2009; Liu et al., 2013; Tanaka, 2003). Moreover, not all tissues of the salamander regenerate as its limb does despite the same genetic toolbox available throughout the individual. Often the regenerative capacities gradually fade out from embryonic stages toward adulthood (Brockes & Kumar, 2005). Since the same cause, amputation, triggers two different fates (scar formation vs. regeneration) in closely related species, in different tissues of the same individual and embryonic versus adult tissue of the same organism, this decision can be viewed as a switch on a largely invariant hardware (Fig. 10.1A). This switch can be tuned by quantitative parameter changes within the regulatory system of the whole tissue. Therein, complex signaling networks including feedback loops play an important role and bridge across spatial scales from signaling molecules to tissue mechanics.

Figure 10.1—Cont'd only close the wound with a scar. Hence the same regulatory systems may be tuned differently to arrive at opposite decisions. (B–E) Epimorphic responses modeled by the continuum approach. (B) Switch from steady-state cell density to exponential growth at time $t_a = 5$ days (mimicking the response to amputation) by keeping the differentiation rate $d = constant$ and increasing the proliferation rate r from $r_0 = 0.2$ to $r_1 = 0.5$ day^{-1}, corresponding to a shortening of the cell cycle from $T_{c0} = 3.5$ to $T_{c1} = 1.4$ days (see Eqs. 1–5). (C) Same as (B) but without changing the proliferation rate r and instead stopping differentiation ($d = 0$). Again, the "tissue" responds with exponential growth (Eq. 4). (D) It is assumed that amputation at time 0 induces a logistic growth with carrying capacity of the population $K = 900$ cells, as indicated (see Eq. 9). (E) Apoptosis modeled as a linear decay process with a decay rate $a = 0.02$ day^{-1} yields exponentially decaying cell density (see Eqs. 10–11). In (B–E) the initial number of cells N_0 is chosen to be 100. (F–H) Mechanisms related to morphallaxis. (F) Random cell migration modeled as cell density diffusion in a one-dimension space (see Eq. 13–14). (G) Directed cell migration driven by chemotaxis. The N cells can diffuse in a one-dimensional space and are guided by the gradient of the concentration $C(x,t)$ of a biochemical signal. (H) The signal C is produced by the cells, diffuses freely, and undergoes linear degradation (see Eqs. 16–19). The initial state is a homogeneous distribution of cells (G) and a peak of signal in the center of the domain (H). Zero-flux boundary conditions have been applied in (F, G, H).

These regulatory and quantitative aspects of regenerative processes remain poorly understood but we can now harness a complementary perspective. The integration of experiments with mathematical models enables us to gain mechanistic understanding of complex systems (Epstein, 2008; Fletcher, 2011; Murray, 2002, 2003). The scientific process of model development integrates and orders the wealth of experimental evidence, knowledge, and data with the goal to generate a comprehensive mechanistic understanding of complex processes. Hence the mathematical model is a tool, not the goal itself, in an iterative and interdisciplinary process. Mathematical modeling also entails the critical assessment of relevant versus less relevant system variables and regulatory interactions. Each mathematical model component is precisely defined and can be monitored during analytical or numerical model analysis, and each component can be modified or perturbed in any desired manner. Simulating a mathematical model corresponds to *in silico* experimentation and unfolds predictive power.

An example for the successful integration of experimentation and mathematical modeling is the seminal work by Hodgkin and Huxley (Hodgkin & Huxley, 1952). By measuring the axonal membrane depolarization under different conditions and linking these different observations with the help of a single mathematical model, they inferred the essential gating properties of ion channels before these molecules themselves had been identified. This ground-breaking work was then extended by many others, notably Noble and coworkers developing a comprehensive model of the heart including tissue mechanics and detailed kinetics of the ion channels in several cell types (Noble, 1962, 2002). During this incremental model development, there coexisted multiple contradicting hypotheses and quantitative comparison of model predictions to experiments resolved many of these disputes.

Hence mathematical modeling is also a powerful tool for rigorously testing and excluding hypotheses. Moreover, mathematical modeling can identify some experimental observations as the inevitable consequence of other pieces of evidence. This approach can also reveal the presently unobservable that is too fast, too slow, too small, too big, too few, or too many for today's measurement technologies. For developmental and cellular processes, there are already many examples where deeper understanding was enabled through mathematical modeling (examples include Brusch, Lorenz, Or-Guil, Bär, & Kummer, 2002; de Back, Zhou, & Brusch, 2013; del Conte-Zerial et al., 2008; Foret et al., 2012; Gierer & Meinhardt, 1972; Käfer, Hayashi, Marée, Carthew, & Graner, 2007; Merks, Glazier, Brodsky, Goligorksy, & Newman, 2006; Nakakuki et al., 2010; Schröter

et al., 2012; Starruß et al., 2012; for recent reviews, see Kondo & Miura, 2010; Lewis, 2008; Meinhardt, 2012; Oates, Gorfinkiel, Gonzalez-Gaitan, & Heisenberg, 2009; Tomlin & Axelrod, 2007). Comparatively fewer mathematical models have been developed for regenerative processes of animals so far. These mathematical models and the insights they provided form the core of this review.

This review is structured along the three phases of regeneration: (1) initiation of a regenerative response, with a systematic comparison of mechanisms that expand the regenerate; (2) tissue patterning during regenerate growth, with a focus on basic pattern formation mechanisms and their implications in organizer regeneration; (3) arresting the regeneration response when the lost tissue portion has been replaced, requiring a tissue-size sensing mechanism that works for initial tissue loss of unpredictable size and at unpredictable locations. We discuss selected results from mathematical models of regeneration processes and highlight the opportunities of extensions of models of developmental processes toward the study of related regeneration processes. We then list open problems for which we expect, during the coming years, substantial progress through the interdisciplinary application of mathematical models.

2. MODELS FOR THE INITIATION OF A REGENERATIVE RESPONSE

2.1. Epimorphosis versus morphallaxis

Successful tissue regeneration implies that the injured region, as the most basic of many aspects, restores its cell number. From a naïve perspective, there are three possible and general mechanisms to accomplish that: (1) by inducing proliferation of the preexisting cells close to the amputation plane, (2) by inducing migration of cells coming from noninjured areas, or (3) by reducing the loss of proliferating cells through differentiation and apoptosis close to the amputation plane. Essentially, the first mechanism is known as *epimorphosis* while the second one, if only differentiated noncycling cells would respond, is called *morphallaxis* (Agata, Saito, & Nakajima, 2007). If cycling cells migrate into the regenerate then we speak of epimorphosis again. It is reasonable to assume that proliferation and apoptosis balance each other under homeostatic conditions, that is, before the amputation. Since cell death inhibition leads to a net cell number increase, the third mechanism above could be classified as another case of epimorphosis. Interestingly, this last mechanism is apparently not exploited by nature. On the contrary, it was demonstrated that apoptosis is

actually enhanced after head amputation in *Hydra* and it is necessary to regenerate the missing head after mid-gastric bisection (Chera et al., 2009). Analogously, in mice apoptosis would be activated to promote wound healing and tissue regeneration via the so-called phoenix rising pathway (Li et al., 2010).

To mimic the regenerative response, a realistic mathematical model has to include the possibility of involving either epimorphosis or morphallaxis. In particular, cell proliferation and migration as well as cell differentiation and apoptosis should be considered.

2.2. Modeling cell proliferation, differentiation, apoptosis, and migration

The process of epimorphosis can be attributed to a number of stem cells whose proliferation is activated. A simple mathematical model describing stem cell proliferation and differentiation is

$$\frac{\mathrm{d}N}{\mathrm{d}t} = rN - \mathrm{d}N, \tag{10.1}$$

where $N(t)$ is the density of proliferating cells within some volume at time t, r is the proliferation rate (defined as the rate of total cell number increase divided by the number of proliferating cells), and d is the differentiation rate (defined as the rate of differentiated cell number increase divided by the number of proliferating cells). The following initial condition is chosen:

$$N(t=0) = N_0. \tag{10.2}$$

The proliferation rate r can in a first attempt be approximated as a constant r_0 in homeostatic conditions that increases immediately after amputation (at time t_a) and remains constant afterwards:

$$\begin{aligned} r &= r_0 = d \quad \text{if } t < t_a \\ r &= r_1 > d \quad \text{if} \geq t_a, \end{aligned} \tag{10.3}$$

where $r_1 > r_0$. The differential equation (Eq. 10.1) can be easily solved to obtain the expected homeostasis before amputation and exponential growth expression after amputation (Fig. 10.1B):

$$\begin{aligned} N(t) &= N_0 \mathrm{e}^{(r_0 - d)t} = N_0 \quad \text{if } t < t_a \\ N(t) &= N_0 \mathrm{e}^{(r_1 - d)(t - t_a)} \quad \text{if} \geq t_a. \end{aligned} \tag{10.4}$$

An alternative for increasing the cell number without speeding up the cell cycle, that is, $r = r_0 = r_1$, is to stop to differentiate cells ($d = 0$ after amputation) and let newly formed stem cells proliferate further. Then again, the homeostatic state with constant cell number turns into an exponential growth phase where $N = N_0 e^{r(t-t_a)}$ (Fig. 10.1C). These two models describe the behavior of a number of cells which all divide exactly at the same rate r. From the exponential cell number expression, the cell cycle length T_C is straightforwardly extracted:

$$T_C = \frac{\ln(2)}{r} \tag{10.5}$$

This quantity can be experimentally estimated by means of Bromodeoxyuridine (BrdU) labeling. This methodology involves a synthetic nucleoside analogue of thymidine that can be incorporated into replicating cells during S phase of the cell cycle. The cell cycle length is extracted from the experiments of BrdU labeling by means of a mathematical model proposed more than 20 years ago (Nowakowski, Lewin, & Miller, 1989). The standard model assumes that all the cells divide with the same rate; that is, they constitute a homogenous growing population. The model has been applied to characterize cell proliferation during nervous system development (Gonsalvez et al., 2013) as well as adult neurogenesis (Ponti et al., 2013) to mention just two recent examples.

The model described by Eq. (10.1) implies that all the cells proliferate with the same proliferation rate r. It could be the case that the tissue is composed by different cell subpopulations differing precisely in this parameter and in the initial conditions. For instance, tissue amputation could activate the proliferation of n different cell subpopulations:

$$N = N_1 + N_2 + \cdots + N_n \tag{10.6}$$

And each of them could proliferate ruled by the following equations:

$$\frac{dN_i}{dt} = r_i N_i \tag{10.7}$$

$$N_i(t=0) = N_{i0} \tag{10.8}$$

Not all the cell subpopulations would equally contribute to the overall proliferation kinetics induced by the amputation, this being controlled by the proliferation rates and the initial conditions.

According to the model, once the amputation is performed, each cell subpopulation starts to grow exponentially. But this assumes that there is no impediment related to the space or to the availability of resources. If this would be the case, a logistic growth model can be applied for each subpopulation:

$$\frac{dN_i}{dt} = r_i\left(1 - \frac{N_i}{K_i}\right)N_i \tag{10.9}$$

where the constants K_i represent the carrying capacity of the medium for each subpopulation i. Once each subpopulation size approaches its carrying capacity, the growth velocity shrinks (Fig. 10.1D). This model was successfully applied in many fields including ecology (Sibly, Barker, Denham, Hone, & Pagel, 2005) as well as microbiology (Brusca, Irastorza, Cattoni, Ozu, & Chara, 2013) among many others.

The processes of stem cell proliferation and differentiation were considered in mathematical models of the hematopoietic system (Marciniak-Czochra, Stiehl, Ho, Jäger, & Wagner, 2009; Nakata, Getto, Marciniak-Czochra, & Alarcón, 2012; van der Wath, Wilson, Laurenti, Trumpp, & Liò, 2009). In these models, there is a term working as a "sink" in the stem cell compartment which is equal to a corresponding term conceived as a "source" in the multipotent progenitor cells. The "sink" corresponding to the stem cell differentiation is mathematically analogous to a process of cell death. Indeed, the process of apoptosis of differentiated cells can also be modeled as a first-order decay process:

$$\frac{dN_i}{dt} = -a_i N_i, \tag{10.10}$$

where a_i is the apoptosis rate of cell subpopulation i. The solution of this equation is again straightforward (Fig. 10.1E):

$$N_i(t) = N_{i0}e^{-a_i t} \tag{10.11}$$

Considering proliferation (with logistic growth) and apoptosis together yields:

$$\frac{dN_i}{dt} = r_i\left(1 - \frac{N_i}{K_i}\right)N_i - a_i N_i \tag{10.12}$$

If the density of proliferating cells is much smaller than their carrying capacity then the logistic expression converges to Eq. (10.7) in which the

parameters r_i of this expression correspond to $r_i - a_i$ of Eq. (10.12). Therefore, proliferation, differentiation, and apoptosis can all be accounted for by the same simple expression in the continuum formalism for the cell density.

The previous ordinary differential equations constitute deterministic models of stem cell proliferation and differentiation as well as apoptosis of differentiated cells. N, the cell density, represents the *average* density of stem cells and progenitors which may change or not in time and/or space. When spatiotemporal experimental information of stem cells and progenitors is available, stochastic modeling had demonstrated to be an interesting alternative. For instance, by assuming subpopulations of stem cells stochastically dividing by symmetric or asymmetric cell division, Simons and coworkers could explain tissue homeostasis of intestinal crypt (Snippert et al., 2010), esophageal epithelium repair (Doupé et al., 2012), as well as the clonal distribution of retina (He et al., 2012).

As mentioned earlier, amputation could induce epimorphosis but also morphallaxis. The involved process of random cell migration (for directed migration, see below) in a continuous formalism can be modeled as diffusion of cell density N (Murray, 2002):

$$\frac{\mathrm{d}N}{\mathrm{d}t} = D\frac{\partial^2 N}{\partial x^2}, \tag{10.13}$$

where the parameter D is the diffusion coefficient of the moving cells and is related to the mean squared displacement of cell trajectories. The model predicts that cells that are initially restricted to a localized spatial region will spread over the whole space. In the continuous framework, the initial condition could be modeled, for instance, by a Gaussian distribution:

$$N(t=0,x) = A\mathrm{e}^{(x-\mu)^2/\sigma^2} \tag{10.14}$$

The relevant parameters of the initial condition are μ and σ, the location and the width of the spatial distribution with approximately 95% of the cell population being localized between $\mu - 2\sigma$ and $\mu + 2\sigma$. The spatial distribution of N, which initially started as a narrow distribution with a ratio μ/σ higher than one disseminates all over the space (Fig. 10.1F) and concomitantly decreases this ratio. In the same vein than what was discussed for proliferating cells, this model can be generalized by assuming more than one subpopulation of motile cells, each one characterized by a diffusion coefficient D_i:

$$\frac{dN_i}{dt} = D_i \frac{\partial^2 N_i}{\partial x^2} \tag{10.15}$$

In the framework of regeneration, this model can be applied to explain how the reduction in the cell number in the wound induces a movement of cells coming from the remaining cells in the neighboring (and more populated) regions.

Another interesting possibility is to assume that cells migrate by chemotaxis, for example, guided by the gradient of a chemical factor (Murray, 2002):

$$\frac{dN}{dt} = D_N \frac{\partial^2 N}{\partial x^2} - \alpha \frac{\partial}{\partial x}\left(N \frac{\partial C}{\partial x}\right) \tag{10.16}$$

$$\frac{dC}{dt} = hN - kC + D_C \frac{\partial^2 C}{\partial x^2} \tag{10.17}$$

The model considers a signaling molecule of concentration $C(x)$ which is produced by the cells N(x). The cells are able to diffuse, as in the previous model, and the parameter controlling this process is the cell diffusion coefficient D_N (first term of the right-hand side of Eq. 10.16). The signal is produced at a rate which is proportional to the number of cells N, is linearly degraded and follows diffusion (first, second, and third term of the right-hand side of Eq. (10.17), respectively). The interesting feature of the model can be found in the second term of the right-hand side of Eq. (10.16). This term encodes the chemotactic behavior: the cells distribute over space driven by the spatial gradient of C and controlled by the parameter α. Therefore, the "flux" of chemoattracted cells is maximal where the spatial gradient also shows a maximum. By starting with the following initial conditions:

$$C(t=0,\ x) = A e^{(x-\mu)^2/\sigma^2} \tag{10.18}$$

$$N(t=0,\ x) = N_0, \tag{10.19}$$

the cells "follow" the gradient of C. Hence, the cells orient forming a spatial pattern although they started homogeneously distributed. Figure 10.1G and H shows how the initial signal distribution widens due to diffusion but then approaches a stationary profile as the attracted cells provide a localized source of further signal. The neighborhood of the cell aggregate is depleted of cells and cell density remains unchanged at distances larger than $\sqrt{D_C/k}$ where the signal has decayed. The homogeneous state is stable for large enough D_N.

As mentioned, the initiation of the regenerative response involves cell proliferation, differentiation, apoptosis, and cell migration as the key cellular processes. All of them were included in the models containing systems of ordinary or partial differential equations shown in this section. This continuous approach also plays an important role in the so-called reaction–diffusion models (RDMs) of organizer regeneration discussed in the next section.

3. MODELS FOR TISSUE PATTERNING DURING REGENERATE GROWTH

Nonmathematical as well as mathematical models were proposed to understand the process of tissue patterning during regenerate growth. Among the first class, the polar coordinate model (PCM) was a very influential model proposed to understand the process of regeneration (and specially the role of intercalation) in insect imaginal discs, insect legs, and amphibian limbs (Bryant, French, & Bryant, 1981; French, Bryant, & Bryant, 1976; reviewed in Nacu & Tanaka, 2011). As a step from the first into the second class, Meinhardt developed the mechanistic boundary model that yields the PCM-rules en passant (Meinhardt, 1983). Mathematical models of pattern formation have traditionally received much attention (Gierer & Meinhardt, 1972; Kondo & Miura, 2010; Meinhardt, 1982; Murray, 2003; Turing, 1952). Whereas the fundamental principles appear rather well understood today, we still lack a one-to-one correspondence between essential components in the theory of pattern formation and specific sets of molecules and genes. The latter is slowly emerging from studies of particular model organisms as *Hydra* and planaria as well as mammalian organs. Another well-studied system of embryonic development, the *Drosophila* wing imaginal disc, is now also moving into the focus of regeneration studies (Martín, Herrera, & Morata, 2009). Salamander limbs have attracted significant modeling efforts (reviewed in Newman et al., 2008; Nacu & Tanaka, 2011). In this section, after emphasizing the role of spatial scales for molecular positioning systems, the contributions of the so-called RDMs of organizer regeneration are discussed, with special emphasis on the Gierer–Meinhardt model in the context of *Hydra* regeneration (Gierer & Meinhardt, 1972; Meinhardt, 1982). While these continuum approaches have proven successful as descriptions for density patterns of cells and molecules, cell-based models allow to incorporate and infer additional cellular properties including cell polarity, cell shape, and cell mechanics (Deutsch & Dormann, 2005). We end this section showing how

such a cell-based model has been used to elucidate the mechanisms responsible for liver regeneration in mice after intoxication with a prototypical inducer of pericentral liver damage (Höhme et al., 2010, 2007).

3.1. Embryological versus regeneration spatial scales, Crick's diffusion estimation

Based on the works of Wolpert (Wolpert, 1969) and Child (Child, 1941), Crick highlighted the role of diffusion in embryogenesis by putting forward the Source–Sink model (Crick, 1970). He considered a simple one-dimensional model constituted by a linear array of n spherical cells, each of diameter d (Fig. 10.2). Additional important model assumptions are:

(1) The first cell on the left works as "source" of a certain biochemical signal while the cell, with number n, on the right constitutes a "sink" of this signal.

(2) The diffusion coefficient of the signal of low molecular weight (such as ATP) in an aqueous medium would be $D \sim 2.7 \times 10^{-7}$ cm^2 s^{-1}.

(3) The time t needed to set up a signal gradient would be about 3 h (close to the time suggested by Wolpert).

Crick calculated n, the number of cells constituting the line, as follows:

$$n = \frac{\sqrt{2\,tD}}{d} \tag{10.20}$$

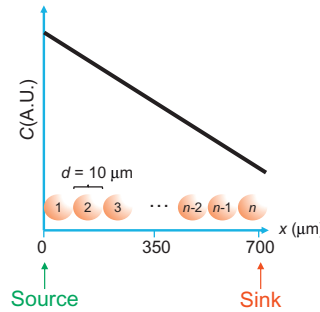

Figure 10.2 *Source–Sink model.* The model, proposed by Francis Crick in 1970, considers a putative morphogenetic signal at concentration C produced by a source located at $x = 0$ and degraded by a sink at the opposite boundary ($x = 700$). A linear array of n cells of diameter $d = 10$ μm is considered. By analyzing this model, Francis Crick showed that diffusion can play an important role in embryonic development. *The figure has been reprinted and modified, with permission, from Crick (1970).*

If the cell diameter d is 10 μm, the line would be covered by $n = 70$ cells. More than four decades later, the idea is still appealing (Schier & Needleman, 2009). Indeed, although morphogens like Wnt have a molecular weight higher than 30 kD which could change the diffusion coefficient and, consequently, the number of cells involved (Shimizu, 2012) the simplicity of the above calculus is remarkable. Independent arguments on the necessary balance between gradient precision and robustness argue for the same number of cells spanning the gradient (Lander, Lo, Nie, & Wan, 2009). Moreover, experimental evidence for Fgf8 morphogen gradients in living zebrafish embryos supported Crick's idea qualitatively, where the "sink" in the zebrafish example corresponds to the signal-receiving/endocytosing cells (Yu et al., 2009).

The success of the Source–Sink model implies that a diffusive mechanism is *sufficient* to explain the establishment of morphogenetic gradients in embryonic development. Could this model be useful to understand the processes of regeneration? In principle, the distances and the times involved in regeneration seem to be higher than those implicated in development. Hence, although diffusion of signaling molecules could play an important role in regenerative processes, other mechanisms should as well be considered.

3.2. RDM of organizer regeneration

A fundamental and widely applied model of self-organizing and regenerating tissue patterns is the RDM. The RDM encompasses coupled positive and negative feedback loops in reaction systems or signaling systems which can dynamically self-organize spatial patterns starting from random initial distributions of the components given different ranges of their spatial influence (Gierer & Meinhardt, 1872; Kondo & Miura, 2010; Meinhardt, 1982; Meinhardt, 2008; Turing, 1952).

A typical example of the RDM with two coupled components is defined by two partial differential equations

$$\frac{\mathrm{d}u}{\mathrm{d}t} = f(u, v) + D_u \frac{\partial^2 u}{\partial x^2} \tag{10.21}$$

$$\frac{\mathrm{d}v}{\mathrm{d}t} = g(u, v) + D_v \frac{\partial^2 v}{\partial x^2} \tag{10.22}$$

where $u(x,t)$ and $v(x,t)$ represent the concentrations of two biochemical species, which react according to the arbitrary functions $f(u,v)$ and $g(u,v)$ of the two concentrations and which diffuse with the diffusion coefficients D_u and D_v. The two reaction terms $f(u,v)$ and $g(u,v)$ capture in a lumped or abstract

manner how a possibly long reaction or signaling pathway regulates u and v in response to the state of u and v.

A version of the RDM with linear functions $f(u,v)$ and $g(u,v)$ was proposed and studied analytically and numerically by Turing (Turing, 1952). He discovered the productive role of diffusion for the self-organization of spatial patterns from random initial distributions and derived a quantitative criterion for the onset of pattern formation as a function of reaction rates and diffusion constants, Eq. 10.23. Turing focused on the instability of a homogeneous system toward periodic patterns, not on the self-organization of monotonous gradients. Also, the properties of the self-organized stationary pattern were not in the focus of this seminal work and could not be studied in this linear version of the RDM since they are determined by the nonlinearities, for example, saturation due to Michaelis–Menten or Hill kinetics or non-linear inhibitor feedback. Since his focus was not on the steady state pattern, Turing did not yet address the following question of pattern regeneration.

Twenty years later, Gierer and Meinhardt developed a nonlinear RDM and numerically studied the properties of self-organizing stationary and dynamic patterns (Gierer & Meinhardt, 1972; Meinhardt, 1982). They discovered that any pattern-forming RDM can be classified as either activator–inhibitor (AI) or activator–substrate-depletion (AS) type. In the AI type, one component has to autocatalytically enhance its own production and is called activator whereas a second component called inhibitor is produced in response to activator presence and suppresses further activator production. In case the inhibitor could not dilute due to transport away from the activator location then a small initial activator elevation would be damped back to the homogeneous state. In the opposite case, the activator will grow at that location until dilution and nonlinear reaction saturation will stop further growth. In the AS type, the autocatalytic component consumes the substrate. Concurrent lack of substrate will damp the activator elevation back to the homogeneous state if the substrate in the neighborhood would not be mobile enough to enter the activator location. Hence, both types are closely related, possess nested positive and negative feedback loops, and depend critically on the diffusion constant of the second component. Meinhardt has successfully applied the RDM to several regeneration scenarios including *Hydra* (see Section 3.3 for a particular example) and planarian regeneration and could explain a number of complex phenotypes (Meinhardt, 1982).

Turing's quantitative instability criterion

$$\frac{D_v}{D_u} > \frac{\left(\sqrt{f_u g_v - f_v g_u} + \sqrt{-f_v g_u}\right)^2}{\left(f_u\right)^2} \tag{10.23}$$

predicts exactly how much faster the inhibitor or substrate has to diffuse than the activator for the activator elevation to persist. The abbreviations f_u, g_u, f_v, and g_v refer to the rates, that is, first derivatives, with which the functions $f(u,v)$ and $g(u,v)$ change when u and v are changed, respectively. These four quantities have to be evaluated for the values u and v that correspond to the unstable homogeneous stationary state. Thus these four quantities become functions of the model parameters and hence a parameter shift can induce or suppress the instability of the homogeneous state toward a heterogeneous pattern. Letting the system evolve from the unstable state, the neighborhood of the emerging activator elevation then receives so much inhibitor, or depletes its substrate, that another activator elevation gets its chance only at large enough distance from the first. The minimal distance between activator elevations, or pattern wavelength for periodic arrangements, was predicted by Turing:

$$l = 2\pi \left(\frac{f_u}{2D_u} + \frac{g_v}{2D_v} \right)^{-1/2} \tag{10.24}$$

This characteristic length scale l of the self-organizing pattern is solely determined by the properties of the two components and independent of the geometry, size, and boundary conditions of the spatial domain in which the RDM is contained. Those domain properties will however determine how many, if any, activator elevations can be accommodated within that domain.

A variant of the RDM with *bistable* local kinetics (introduced in Meinhardt, 1972) and conservation of the total amount of one component within the domain has been analyzed by Edelstein-Keshet and coworkers (Mori, Jilkine, & Edelstein-Keshet, 2008). Therein a superthreshold perturbation of the homogeneous state is required to excite the coexisting bistable state. A front will extend the spatial region of the excited state until the consumption of the conserved component halts the front, termed wave pinning (Mori et al., 2008). This pattern-forming mechanism is fundamentally different from the linear instability mechanism and could underlie those systems that require a superthreshold stimulus for regeneration. Pattern formation in such multistable systems could be triggered by additional directed transport processes, including cell flow and advection of molecules. Examples of these coupled mechanochemical systems have been reviewed in Howard, Grill, and Bois (2011).

The concept of the RDM has helped to understand the formation and spatial localization of organizers, that is, localized signaling centers, during

embryonic development (Kondo & Miura, 2010; Meinhardt, 1982; Murray, 2003). Starting from an unpatterned cell mass, the temporal dynamics of a RDM can establish an organizer in a field of otherwise low activity. As discussed next, these predictions describe aspects of *Hydra* regeneration from fragments of the body column (Meinhardt, 1982) or from dissociated and reaggregated cells (Hobmayer et al., 2000; Technau et al., 2000).

3.3. Gierer-Meinhardt model of hydra regeneration

As mentioned in the introduction, after the initiation of the regenerative response, tissue patterning processes during regenerate growth are generated. The RDM developed by Gierer and Meinhardt (Gierer & Meinhardt, 1972; Meinhardt, 2008) can describe the process of pattern formation needed in regeneration. In particular, this model describes many features observed in the regenerating *Hydra* by involving two biochemical signals A and H, both able to diffuse over a one-dimensional space (representing the head–foot axis of *Hydra*). The first signal, the activator A, is upregulating its own production while it is inhibited by the second signal H (from the German word *Hemmstoff*, for inhibitor). The model differential equations look like:

$$\frac{\mathrm{d}A}{\mathrm{d}t} = \frac{\rho A^2}{H} - \mu_A A + D_A \frac{\partial^2 A}{\partial x^2} + \rho_A \tag{10.25}$$

$$\frac{\mathrm{d}H}{\mathrm{d}t} = \rho A^2 - \mu_H H + D_H \frac{\partial^2 H}{\partial x^2} \tag{10.26}$$

The model describes a process by which both, the activator and the inhibitor are upregulated by a nonlinear autocatalytic production term A^2 (first term of the right-hand side of Eqs. 10.25 and 10.26) and linearly degraded with rate constants μ_A and μ_H (second term of the right-hand side of Eqs. 10.25 and 10.26). Additionally, both signals are able to diffuse with diffusion coefficients D_A and D_H (third term of the right-hand side of Eqs. 10.25 and 10.26) and the inhibitor is downregulating the activator production (first term of the right-hand side of Eq. 10.25). The self-enhancement of the activator is not linear in order to overcome the linear degradation. This condition is compatible with an activator working only in a dimeric configuration. The factor ρ is the *source density* or *competence* and describes the cells' ability to promote the self-enhancement of the activator.

Starting from a homogenous initial condition (i.e., both the activator and the inhibitor are homogenously distributed in the space) a stable spatial

pattern is formed if the inhibitor distributes faster and has a more rapid turnover than the activator ($D_H > D_A$ and $\mu_H > \mu_A$, respectively). Parameter ρ_A (Eq. 10.25) is one of the regeneration keys and is responsible for the production of activator which is independent of the activator itself. When *Hydra* amputation is mimicked by removing the activator from a region of the space, this parameter allows that new activator is produced there (Fig. 10.3A–C).

Experimental evidence indicates that *Hydra* fragments from all positions are capable to regenerate a new polyp. The model can reproduce this phenomenon by assuming that the source density is enhanced by the activator, while undergoing a linear degradation, diffusion, and also showing an activator-independent production, as it is encoded in the following expression:

$$\frac{d\rho}{dt} = \gamma_\rho A - \mu_\rho \rho + D_\rho \frac{\partial^2 \rho}{\partial x^2} + \rho_\rho \tag{10.27}$$

If the inhibitor has a small time constant (allowing the reappearance of the new organizer immediately after the original organizer removal) while the source density has a larger one, then, the organizing region inhibits the formation of other competing organizing regions at short times while inducing a new organizing region at that position closest to an amputated organizing region.

The specific RDM of Eqs. (10.25) and (10.26) is also capable of establishing an organizer *de novo* from unpatterned cell aggregates as described in the previous section and as it has been observed in experiments with dissociated cells of *Hydra* (Hobmayer et al., 2000; Technau et al., 2000). This self-organization process can be illustrated by simulating Eqs. (10.25) and (10.26) on a spatial domain with the same shape as the reported cell aggregate. For suitably chosen parameter values four organizers forming *de novo* can be observed, as in the mentioned experiments (Fig. 10.3D–F, and Supplementary Material, http://dx.doi.org/10.1016/B978-0-12-391498-9.00011-5). In this simulation, the particular shape of the aggregate differs from a circle, which is isotropic, and hence the shape triggered the break of angular symmetry such that the organizers could place themselves at large enough distance to each other. If coupled to cell migration upward the gradients of u or v, then the RDM would also let the experimentally observed aggregate shape emerge from an initially circular aggregate shape. Such bidirectional coupling of a pattern forming RDM with shape dynamics has been introduced as morphodynamics (Salazar-Ciudad, Jernvall, &

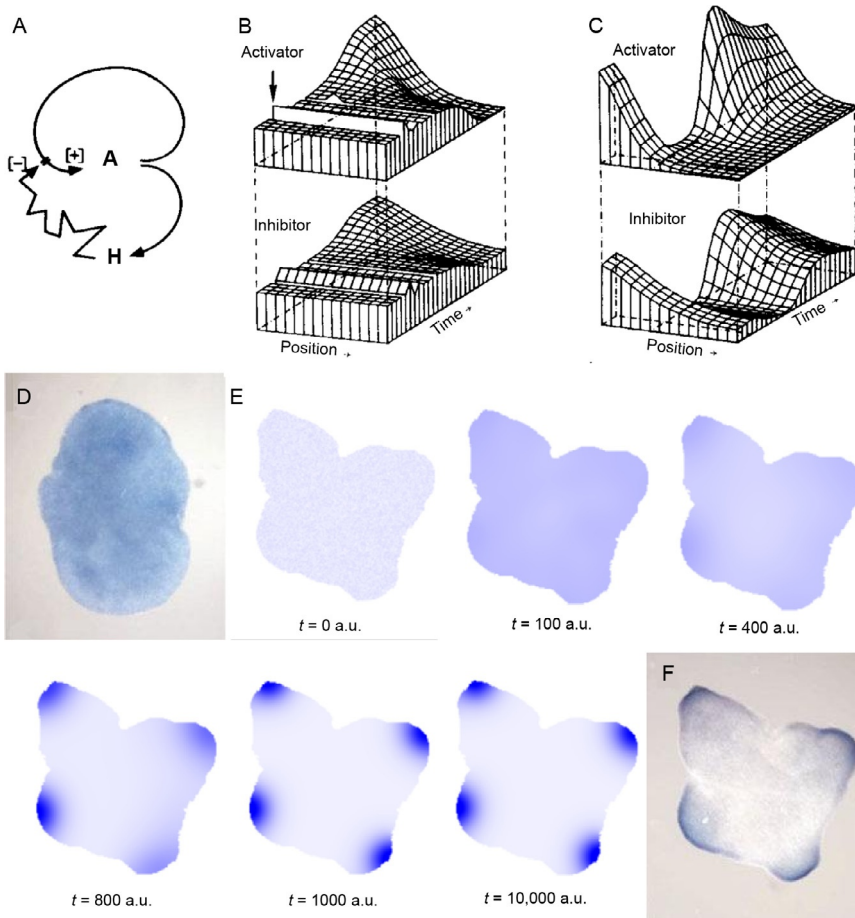

Figure 10.3 *Activator–Inhibitor model*. (A) Model diagram of activator (*A*) and inhibitor (*H*) components linked by positive and negative regulatory interactions (see Eqs. 10.25–10.26). (B) Space–time profiles of simulated activator and inhibitor dynamics under normal developmental conditions. Starting from homogenous concentrations of both components, the one-dimensional "tissue" self-organizes a pattern in which the activator is concentrated at the left border. (C) Simulation results for the regeneration condition with identical parameter values as in (B) but removing the activator peak after the initial three time steps. The "tissue" regenerates the original pattern (Meinhardt, 1982). (D) Experimental confirmation of the homogeneous initial distribution of the head marker HyTcf shown by hybridization 24 h after plating a *Hydra* cell aggregate. (E) Time course of the activator–inhibitor model of (A–C) simulated on a two-dimensional spatial domain which was trimmed to the shape of the experimental *Hydra* cell reaggregate reported in Hobmayer et al. (2000) and shown in (F). The spatial distribution of the activator variable is represented by a color scale with maximum 10 and darker color denoting larger values. Starting from homogeneous initial conditions with

(*Continued*)

Newman, 2003). For a perfectly circular aggregate, tiny density fluctuations would get amplified and break the angular symmetry spontaneously. It has also been reported that spheroids of reaggregated *Hydra* cells may undergo osmosis-driven shape oscillations that provide a symmetry break (Kücken, Soriano, Pullarkat, Ott, & Nicola, 2008). As a model prediction, a small guidance cue like a fraction of an organizer could be used to place the new organizer at a desired position.

The various RDMs are able to explain processes of tissue pattern formation and self-organization, reproducing many phenomena observed during embryonic development and regeneration. While these RDMs describe density patterns of cells and molecules, cell-based models have allowed the inference of cell properties such as the orientation of the division axis. The next section demonstrates this complementary approach.

3.4. Cell-based model of liver regeneration

The extraordinary regeneration capacity of the mammalian liver had already inspired the fate of Prometheus in Greek Myth. Upon intoxication, dying hepatocytes are replaced by new hepatocytes, largely through proliferation of the remaining hepatocytes (Höhme et al., 2007). One open question is which cues guide the activation of proliferation and transport of newly created hepatocytes such that dead hepatocytes can be replaced without distorting the intact parts of the tissue architecture and the vascular network in particular. Drasdo and coworkers provided a proof of principle that mathematical modeling in combination with microscopy data from confocal laser scans, image segmentation, and three-dimensional tissue reconstruction can be used to address this question (Höhme et al., 2010).

Figure 10.3—Cont'd small added noise, all cells (here lattice nodes) first upregulate the activator and tiny asymmetries amplify until all weaker activator regions become suppressed by the stronger ones' inhibitor. The strong activator regions repel each other and thereby tend to form in or move into corners of the irregular aggregate shape. The similarity between distributions at 10^3 and 10^4 arbitrary time units (a.u.) indicates that a stable state has been reached. An animation of the full simulation with activator (inhibitor) distribution in the left (right) panel is available online as supplementary material, http://dx.doi.org/10.1016/B978-0-12-391498-9.00011-5. The multi-scale modeling and simulation software Morpheus was used as it can account for irregular, image-derived spatial domain shapes (Starruß, de Back, Brusch & Deutsch, 2014). See also Meinhardt (2012) for a similar simulation in a different geometry. (F) Snapshot of HyTcf hybridization at 48 h after plating of the *Hydra* cell aggregate shows the same pattern as in the simulation. *Panels A–C have been reprinted, with permission, from the classic book Meinhardt (1982). Panel D: Image reprinted with permission from Hobmayer et al. (2000). Panel F: Image reprinted with permission from Hobmayer et al. (2000).*

Their microscopy snapshots captured hepatocyte rearrangements at lobule scale during liver regeneration in mice after CCl_4 intoxication. CCl_4 is a prototypical chemical inducing liver damage around central veins. The building blocks of this mathematical model are the image-derived blood vessel network and spheres representing single hepatocytes. Both building blocks are deformable according to force balances that are evaluated at each time step of the simulation. These and the following model components also need to be parameterized and previously published data has instructed most of the parameter choices, for details see (Höhme et al., 2010). Each sphere has the options to migrate, to grow, to divide, or to die and these are executed according to rules that incorporated the configuration within a neighborhood, long-range signals as well as a stochastic component. Defining these rules requires mechanistic insight into the regulation of cell-scale processes during liver regeneration but this mechanistic insight is currently lacking. Several alternative mechanisms were proposed including (1) homogeneous activation of hepatocyte proliferation and hepatocyte displacement due to cell–cell repulsion, (2) directed cell migration toward the necrotic lesion possibly guided by chemoattractants secreted by dying hepatocytes, and (3) the alignment of cell divisions in the direction of the closest blood vessel.

In order to test these competing hypotheses, all of them were implemented as separate models and their emergent tissue-scale behavior simulated. The authors compared the time courses of hepatocyte density, lesion closure, and hepatocyte-vessel contact area between each of the models and the experimental data. After exploring the parameter space of each model, these three emergent properties and the simulated overall tissue architecture were found to be in agreement with the experimental data only for the model corresponding to the aforementioned mechanism number (3) (Fig. 10.4A–E). No other tested mechanism was able to replace the role of daughter cell alignment with blood vessels in these simulations. This model prediction was subsequently tested using independent experimental data. Altogether, this study demonstrated how multiscale mathematical modeling can be used to infer cell-scale properties from tissue-scale experimental observables.

4. MODELS FOR ARRESTING THE REGENERATIVE RESPONSE

4.1. Central versus decentral growth control

During embryonic development and tissue regeneration alike, the individual-specific size of an organ collectively results from parallel,

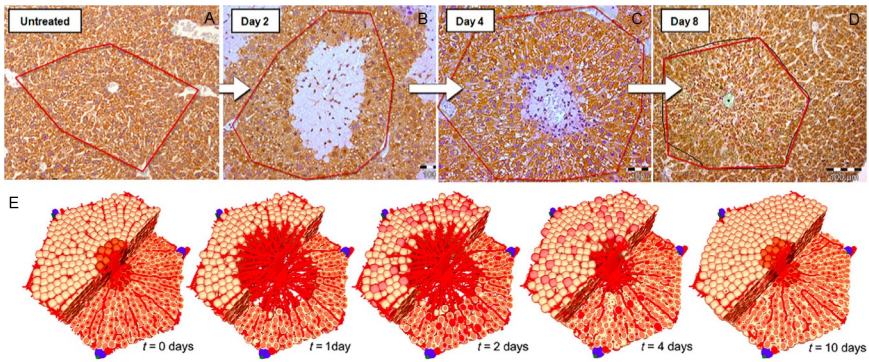

Figure 10.4 *Liver regeneration model.* (A–D) Mouse liver lobules with CCl4 induced liver damage in the central region, visible as gray domain in (B, C). Light microscopy images for (A) Control, (B) 2 days, (C) 4 days, and (D) 8 days after administration of CCl4 illustrate how the liver cell mass regenerates. Lines in (A–D) denote the borders of a single liver lobule in cross section. (E) Simulation of liver regeneration due to liver cell proliferation within a digital liver lobule. *All images reprinted with permission from Höhme et al. (2010).*

decentralized decisions of single cells. Thus, organ size regulation represents a multiscale problem. The single cell's size and shape distributions together with cell number determine organ proportion and macroscopic extension. Thereby, information simply accumulates from the small to the large scale. But how is the information about the instantaneous organ size transferred back to the small scale of single cells where it controls cell proliferation such that the regenerative growth process is arrested once the organ's target size is reached? This question is equally pressing for developmental as well as for regeneration research. Different modes of information transfer and corresponding cellular sensing mechanisms have been studied as part of developmental biology.

(i) Bacterial biofilms employ quorum sensing to evaluate cell density (Ben-Jacob, Cohen, & Levine, 2000). A similar integrative role is played by molecules termed "chalones" in tissues (Lander, Gokoffski, Wan, Nie, & Calof, 2009).

(ii) *Hydra* employs long-range signals to pattern its body column and to bud off daughter polyps when a critical size is exceeded. Such behavior has been reproduced by RDMs (Gierer & Meinhardt, 1972; Meinhardt, 1982). Hence, growth is not arrested but excess tissue will be separated from the completely regenerated tissue.

(iii) The mammalian liver which operates in relation to the organismal metabolic needs seems to be controlled centrally by circulating growth stimuli that reflect organismal demand.

(iv) Embryonic appendage development employs an intrinsic size regulation mechanism until central hormone levels entrain it to organismal size in a later proportional growth phase. The organ-intrinsic growth regulation phenomenon is the most relevant to tissue regeneration in higher organisms and is still controversial today.

We review the competing hypotheses on organ-intrinsic growth regulation and the corresponding models in more detail below. We restrict the survey to those mechanisms implicated in *Drosophila* wing imaginal disc growth, a primary experimental paradigm of tissue size regulation. We emphasize the *central* versus *decentral* nature of each mechanism for organ-intrinsic growth regulation. Since regenerative processes have to cope with a range of diverse starting conditions, any central growth control mechanism needs to deliver the right dose of growth stimulus for the required size increase dependent on the size of the responding tissue and on the geometric relation between stimulus source and responding tissue. Whereas this dosage may be hard-coded in the organizer behavior for a stereotypic developmental process, it would need to be "recomputed" specifically for each instance of damage or amputation. The advantage of a decentral growth control mechanism such as intercalation is that damage sensing and growth response can be linked locally. The mathematical models reviewed in this section, notably the cell-based models, are defined by extended rule sets and parameter sets which we do not describe in full detail here, please see the cited references for these details.

An elegant test of the alternative hypotheses for growth regulation is provided by controlled elimination of groups of cells from the disc. Morata and coworkers have induced apoptosis of cells in the disc either randomly or within clones of transformed cells and observed that the discs regenerate perfectly both from massive cell loss as well as from loss of localized clones (Herrera, Martin, & Morata, 2013; Perez-Garijo, Shlevkov, & Morata, 2009; Repiso, Bergantiños, & Serras, 2013). The apoptotic clones were multiple and induced at random locations within the disc but many repetitions of these experiments with many random combinations of apoptotic clones have consistently yielded the growth arrest at the correct size. From these results we extrapolate to a hypothetical experiment with a single apoptotic clone at a desired location. It is unlikely that this single clone would yield a size defect since all combinations of clone locations resulted in correctly regenerated discs and it is hard to imagine a way in which all the single-clone errors always cancelled out.

For each of the three hypothetical growth regulation mechanisms discussed below, we will use a *Gedanken experiment* with induced cell loss in

a compact region at desired location (e.g., the white sector in Fig. 10.5B) and then derive the model prediction regarding the regenerated disc size. Those models that will predict the recovery of the original disc size are then more likely explanations whereas others that contradict the experimental evidence may apply only to early developmental stages. This argument can be corroborated by quantitative analysis of the mathematical models but this shall be the subject of a separate work.

4.2. Mechanical feedback models

Mechanical forces have been proposed to spread the information about overall tissue geometry within the tissue (Shraiman, 2005). Growth against the peripheral layer of cells will increase the physical pressure within the tissue and can eventually arrest growth at suprathreshold pressures. Amputation would relieve this pressure through small spatial relaxation of the new tissue margin and thereby reactivate proliferation throughout the entire remaining tissue. This closed negative feedback loop of growth-dependent pressure increases and pressure-hindered growth represents a *decentral* mechanism and is called mechanical feedback model (Aegerter-Wilmsen, Aegerter, Hafen, & Basler, 2007; Hufnagel, Teleman, Rouault, Cohen, & Shraiman, 2007). So far, this model has been studied in the context of *Drosophila* wing imaginal disc growth during development. Two slightly different variants of the model have been implemented as a continuum model (Aegerter-Wilmsen et al., 2007) and a cell-based model (Hufnagel et al., 2007), respectively.

The disc is an epithelium with the central part of the wing pouch approximately confined to a planar subspace such that it cannot fold into the third dimension. In the model, proliferation is maintained by and contributes to a particular physical stress distribution that compresses inner regions and tangentially stretches outer cell layers (Fig. 10.5). Coupled to a concentration gradient of diffusible growth stimuli, a homogeneous proliferation rate emerges in model simulations as a new property at the tissue scale without the need to define a unique proliferation rate at the cell scale (Aegerter-Wilmsen et al., 2007; Hufnagel et al., 2007). The final disc size is determined by a balance of heterogeneous growth stimulus, compression, and stretching forces (Fig. 10.5). Growth is arrested since a closed outer belt of cells under stretch (outer/blue areas in Fig. 10.5) encapsulates the inner part of the disc (Aegerter-Wilmsen et al., 2007; Hufnagel et al., 2007). The liver regeneration model discussed in Section 3 is another instance of the mechanical

feedback model since also there proliferation is arrested once the open space of the lesion has been filled with cells and pressure within the tissue arrests further proliferation.

We now consider the above-described Gedanken experiment in analogy to actual disc regeneration experiments (Herrera et al., 2013; Perez-Garijo et al., 2009). If the homeostatic stress distribution is perturbed by cell loss in a sector or a narrow ray near the periphery of the disc (white box in Fig. 10.5B), then the formerly closed outer belt will break open even for small localized damage in that region and the compression of the formerly encapsulated inner tissue will be relieved. This mechanical relaxation response has been observed through changes of the force-dependent optical birefringence of the tissue (Nienhaus, Aegerter-Wilmsen, & Aegerter, 2009). In our Gedanken experiment, proliferation will fill the void in the tissue but it is very unlikely that the newly formed cells in that region would restore the highly stretched configuration of the closed outer belt which is necessary to compress the inner part of the tissue and consequently arrest proliferation. The new cells would rather fill the void in a relaxed

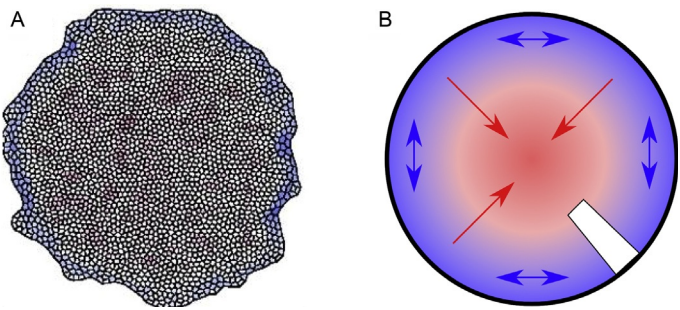

Figure 10.5 *Mechanical feedback model.* (A–B) One of the proposed mechanisms for tissue size regulation combines a *central* growth factor source (not shown) which drives proliferation in the center of the wing disc with a *decentral* mechanical feedback mechanism through proliferation-inhibiting compression forces (radial/red arrows in B for direction and darkness/intensity of red color in the center of A and B for amplitude of forces) and proliferation-promoting stretch forces (tangential/blue arrows in B for direction and darkness/intensity of blue color in the periphery of A and B for amplitude of forces). (A) Snapshot of a cell-based simulation starting from a small and relaxed cell aggregate shows the buildup of the force pattern (Hufnagel et al., 2007). Ongoing growth in the center stretches outer cell layers tangentially which consequently compresses the inner cell mass such that the net proliferation rate decreases sharply at the target size. (B) Sketch of the force pattern and location of the hypothetical tissue loss that is discussed in a Gedanken experiment (see text). *Panel A was reprinted with permission from Hufnagel et al. (2007).*

configuration and growth will continue, thereby starting to stretch the new outer belt, until a new balance at a *larger* disc size can eventually arrest growth. This would not explain the reported disc regeneration with normal size (Herrera et al., 2013; Perez-Garijo et al., 2009). The overgrowth, as wrongly predicted by mechanical feedback models, could be corrected through a more active role of the *central* growth stimulus gradient, as discussed in Aegerter-Wilmsen et al. (2012) and the next section.

4.3. RDMs of growth regulation

The interplay between diffusible growth promoting morphogen gradients (including Decapentaplegic, Dpp) as well as diffusible growth repressing morphogen gradients (including Brinker, Brk) has been studied in great detail (Schwank, Restrepo, & Basler, 2008; Serrano & O'Farrell, 1997; Wartlick, Mumcu, Kicheva, et al., 2011). This mechanism can again be represented by reaction diffusion equations (Meinhardt, 1982). The local balance of the instantaneous concentrations of the antagonistic stimuli could determine the proliferation response during embryonic development (Schwank et al., 2008). A different option is to process the temporal history of concentration changes and let any cell divide when the *relative* stimulus increment since the last division exceeds a threshold, for example, 40–50% as measured for the wing disc (Wartlick, Mumcu, Kicheva, et al., 2011). Then the predicted cell cycle time

$$T_c(t) \sim \left(\frac{1}{C(x,t)} \frac{\partial C(x,t)}{\partial t} \right)^{-1} \tag{10.28}$$

becomes uniform for the observed *scaling* stimulus gradient (Wartlick, Mumcu, Kicheva, et al., 2011). The time dependence of the local stimulus $C(x,t)$ results from a combination of time-dependent stimulus release from the central organizer $C_0(t)$, retardation due to signal propagation between organizer and receiving cell, and displacement of the receiving cell within a stimulus gradient by proliferation of cells between the receiving cell and the organizer. Since the latter proliferation is ruled by Eq. 10.28 and the scaling gradient has the property

$$\frac{1}{C(x,t)} \frac{\partial C(x,t)}{\partial t} = \frac{1}{C_0(t)} \frac{\partial C_0(t)}{\partial t} \tag{10.29}$$

then, after inserting Eq. (10.29) into Eq. (10.28), $T_C(t)$ is determined by the time course $C_0(t)$ of stimulus release from the central organizer.

Both above options constitute *central* mechanisms ruled by the dynamics of the stimulus source(s) and these can well explain the developmental data sets. But in the Gedanken experiment in analogy to real experiments (Herrera et al., 2013; Perez-Garijo et al., 2009), a clone of apoptotic cells far away from the organizer would have to transfer information on the loss of cells within the clone back to the organizer such that an additional impulse $\partial C_0(t)/\partial t$ of growth stimulus can be released. This cannot be excluded but appears to be a difficult requirement for all central growth control mechanisms. The next difficult question would then be how the organizer could integrate damage signals from different wounds throughout the disc.

4.4. Slope sensor models

Using as proliferation trigger the spatial slope of a concentration gradient instead of its local values has been proposed as a simple and robust mechanism for relaying the information of the current tissue size to each cell (Day & Lawrence, 2000; García-Bellido, 2009; García-Bellido and García-Bellido, 1998; Lawrence & Struhl, 1996; Rogulja & Irvine, 2005). If the overall expression profiles interpolate between fixed extreme values at the organ boundaries then the local slope would reflect organ size (Day & Lawrence, 2000; Lawrence & Struhl, 1996). If individual cells locally sense a suprathreshold slope then they might proliferate and intercalate new expression levels such that a shallower slope results (García-Bellido, 2009; García-Bellido and García-Bellido, 1998). This decentral mechanism would arrest developmental disc growth at the target size that has been evolutionarily encoded as the same threshold value in each cell. Each cell may compare this threshold value to a function of its local slope signal and the absolute expression level. This way, either linear or exponential expression gradients, thanks to the constant relative slope of the latter, could serve as input to the slope sensor.

Over the past few years, experimental evidence on the role of Fat and Hippo signaling pathways in disc growth shows that cells indeed sense differences of Dachsous (Ds) and Four-jointed (Fj) levels as compared to their neighboring cells (Reddy & Irvine, 2008; Staley & Irvine, 2012). Both Ds and Fj are expressed as concentric gradients with extremes at the disc margin and center, respectively, but opposite orientation (Rogulja, Rauskolb, & Irvine, 2008). Fat and Ds are large trans-membrane proteins that bind each other whereas Fj is a Golgi-localized kinase that can modulate Fat and Ds

activities (Ishikawa, Takeuchi, Haltiwanger, & Irvine, 2008). A suprathreshold difference of Ds or Fj among neighboring cells inhibits the tumor suppressor Hippo through Fat and thereby activates proliferation (Cho et al., 2006; Rogulja & Irvine, 2005).

In the Gedanken experiment in analogy to real experiments (Herrera et al., 2013; Perez-Garijo et al., 2009), apoptosis of cells anywhere with intermediate expression levels would induce a large slope for cells at the wound margin and correspondingly trigger proliferation until the expression gap has been filled by cells expressing the intermediate levels. Such a system will regenerate the original tissue size as long as the central extreme expression level is retained. This interpolation of expression levels, representing positional values, has been tested in grafting experiments with cricket legs (Bando et al., 2009). If a tissue graft was reinserted in reversed orientation then two large tissue portions of the size of the graft were regenerated until a zig-zag profile of positional values could fulfill the slope threshold criterion everywhere again, as expected from mathematical models (Meinhardt, 1982). Hence, the slope sensor model is an attractive candidate to be considered further.

4.5. Proposed integrated model

The reaction–diffusion and mechanical feedback models can explain many aspects of the developmental processes of *de novo* pattern formation in initially uniform fields of cells (Aegerter-Wilmsen et al., 2012; Meinhardt, 1982; Wartlick, Mumcu, Jülicher, & Gonzalez-Gaitan, 2011). Once established, these patterns can be translated into gradients of cell-bound properties, for example, the expression level of plasma membrane components, as proposed (Lewis & Wolpert, 1976; Slack, 1980) and found experimentally (Rogulja, Rauskolb, & Irvine, 2008). These cell-bound properties can be stably maintained over long time at low cost since they do not diffuse away. Upon cell division, daughter cells could initially establish their own cell-bound properties by averaging over their neighbors' properties and then maintain this once established property (García-Bellido, 2009). Therewith, a growing tissue would maintain a gradient of cell-bound properties. The slope of this gradient would gradually decrease as a result of daughter cells shifting previously neighboring cells with fixed properties further apart. Dachsous expression in the fly imaginal discs and Prod1(CD59) in the newt limb appear to encode such large-scale gradients of cell-bound properties. A slope-sensing mechanism would then inform each cell any time about

the macroscopic tissue extension and proliferation could cease as the slope approaches a target value. This way, multiple mechanisms would be required subsequently and mutagenesis studies of overall growth defects would reveal components of seemingly competing mechanisms.

5. OPEN PROBLEMS

When compared to developmental processes during embryogenesis, two fundamental differences become evident: developmental processes operate (1) on small embryonic length scales and involving hundreds of cells and (2) from defined starting conditions whereas regenerative processes bridge to larger adult length scales involving millions of cells and function from a range of diverse starting conditions. Hence a central question is: Can developmental processes be reinstated and adapted or are there entirely new regenerative processes to be discovered?

So far, the modeling of regenerative processes has often focused on explaining the principles that govern growth control and patterning, basically assuming the responses of only a single cell type. While this may suffice for a system such as the *Drosophila* wing disc, regeneration in other systems including *Hydra* and the salamander limb clearly involve the participation of multiple cell types that retain a separate identity during regeneration (Hobmayer et al., 2012; Kragl et al., 2009). For modeling the dynamics of these coupled populations, it will be important for experimentalists to determine whether the different cell types show common properties, or distinct profiles of cell proliferation, cell death, and migration. From a molecular point of view, it will be important to determine whether one common injury associated signal coordinates the responses of different cell types or multiple signals act in parallel. Finally, the interaction and coordination among the different cell types will also come into play during tissue restoration that will eventually need to be incorporated into models. From a modeling perspective, the integration of cell-based models with continuum approaches (via differential equations) will be necessary to truly integrate the large-scale spatial control of cellular responses and the concrete cellular behaviors that occur.

Interestingly, regeneration occurs over many different spatial scales. For example, small pieces of planaria regenerate to small individuals, while larger pieces regenerate to larger animals. In salamanders, regeneration occurs in small larvae or adults that can be 10 times bigger than the larvae. Therefore,

the mechanisms controlling proliferation and patterning must be robust over different spatial scales. This consideration of size will be an important aspect of evaluating different models and will require experiments in animals of different sizes to help determine how scaling is occurring. In considering scaling, it is likely that regenerating structures have a natural range of scale at which patterning can be completed. Then there should be a second phase of matching the regenerate with overall body size. When this second phase starts and how it is controlled will be fascinating future challenges for biologists and mathematicians alike.

6. CONCLUSIONS AND PERSPECTIVES

Many studies of regenerative processes have provided qualitative mechanistic models or pathway maps. Translating these qualitative models into mathematical models will allow their internal consistency to be verified, to clarify hidden assumptions, and to define the specific conditions and parameter ranges for which the anticipated emergent behavior indeed results. The current blossoming of quantitative experimentation in the regeneration field is providing the foundation to extend the interdisciplinary approach from developmental to regenerative processes and to benefit from mathematical modeling more widely. Mathematical modeling has already contributed to a better understanding of regenerative processes with examples from lower as well as higher organisms and from the three phases of regeneration. (1) Key processes of the initiation phase of a regeneration response can be described by comparatively simple models and the task is now to model the signaling pathways that tune the parameter values of the simple models, thereby extending them. (2) Tissue patterning during regenerate growth is a very attractive and very active research area that benefits from classic and abstract models which now have to be linked to the discovered molecular components. (3) The arrest of the regeneration response through tissue size regulation mechanisms still poses fundamental challenges. Central and decentral regulatory mechanisms appear to operate in sequence such that the latter regulate regenerative processes. However, mathematical modeling needs to accelerate in this area. We hence like to advocate a closer integration of experimentation and mathematical modeling based on an iterative process of model development, model predictions, quantitative experiments, and model refinement.

ACKNOWLEDGMENTS

We are grateful to Salvador Herrera, Fabian Rost, Michael Kücken, Andreas Deutsch, Hans Meinhardt, Kenneth Irvine, Brigitte Galliot, and Gines Morata for fruitful discussions. The authors acknowledge support by the Human Frontier Science Program (HFSP, grant RGP0016/2010), the cluster of excellence cfaed and the German Ministry for Education and Research (BMBF, Grants 0316169A and 0315734).

REFERENCES

Aegerter-Wilmsen, T., Aegerter, C. M., Hafen, E., & Basler, K. (2007). Model for the regulation of size in the wing imaginal disc of Drosophila. *Mechanisms of Development*, *124*, 318–326.

Aegerter-Wilmsen, T., Heimlicher, M. B., Smith, A. C., Barbier de Reuille, P., Smith, R. S., Aegerter, C. M., et al. (2012). Integrating force-sensing and signaling pathways in a model for the regulation of wing imaginal disc size. *Development*, *139*, 3221–3231.

Agata, K., Saito, Y., & Nakajima, E. (2007). Unifying principles of regeneration I: Epimorphosis versus morphallaxis. *Development, Growth & Differentiation*, *49*, 73–78.

Bando, T., Mito, T., Maeda, Y., Nakamura, T., Ito, F., Watanabe, T., et al. (2009). Regulation of leg size and shape by the Dachsous/Fat signalling pathway during regeneration. *Development*, *136*, 2235–2245.

Bely, A. E., & Nyberg, K. G. (2009). Evolution of animal regeneration: Re-emergence of a field. *Trends in Ecology & Evolution*, *25*, 161–170.

Ben-Jacob, E., Cohen, I., & Levine, H. (2000). Cooperative self-organization of microorganisms. *Advances in Physics*, *49*, 395–554.

Binder, P. M. (2008). Frustration in complexity. *Science*, *320*, 322–323.

Birnbaum, K. D., & Sánchez Alvarado, A. (2008). Slicing across kingdoms: Regeneration in plants and animals. *Cell*, *132*, 697–710.

Brockes, J. P., & Kumar, A. (2005). Appendage regeneration in adult vertebrates and implications for regenerative medicine. *Science*, *310*, 1919–1923.

Browne, E. N. (1909). The production of new hydranths in Hydra by the insertion of small grafts. *The Journal of Experimental Zoology*, *7*, 1–13.

Brusca, M. I., Irastorza, R. M., Cattoni, D. I., Ozu, M., & Chara, O. (2013). Mechanisms of interaction between Candida albicans and Streptococcus mutans: An experimental and mathematical modelling study. *Acta Odontologica Scandinavica*, *71*, 416–423.

Brusch, L., Lorenz, W., Or-Guil, M., Bär, M., & Kummer, U. (2002). Fold-Hopf bursting in a model for calcium signal transduction. *Zeitschrift für Physikalische Chemie*, *216*, 487–497.

Bryant, S. V., French, V., & Bryant, P. J. (1981). Distal regeneration and symmetry. *Science*, *212*, 993–1002.

Chera, S., Ghila, L., Dobretz, K., Wenger, Y., Bauer, C., Buzgariu, W., et al. (2009). Apoptotic cells provide an unexpected source of Wnt3 signaling to drive hydra head regeneration. *Developmental Cell*, *17*, 279–289.

Child, C. M. (1941). *Patterns and problems of development*. Chicago: University of Chicago Press.

Cho, E., Feng, Y., Rauskolb, C., Maitra, S., Fehon, R., & Irvine, K. D. (2006). Delineation of a Fat tumor suppressor pathway. *Nature Genetics*, *38*, 1142–1150.

Crick, F. (1970). Diffusion in embryogenesis. *Nature*, *225*, 420–422.

Day, S. J., & Lawrence, P. A. (2000). Measuring dimensions: The regulation of size and shape. *Development*, *127*, 2977–2987.

de Back, W., Zhou, J. X., & Brusch, L. (2013). On the role of lateral stabilization during early patterning in the pancreas. *Journal of the Royal Society Interface*, *10*, 20120766.

del Conte-Zerial, P., Brusch, L., Rink, J., Collinet, C., Kalaidzidis, Y., Zerial, M., et al. (2008). Membrane identity and GTPase cascades regulated by toggle and cut-out switches. *Molecular Systems Biology*, *4*, 206.

Deutsch, A., & Dormann, S. (2005). *Cellular automaton modeling of biological pattern formation: Characterization, applications, and analysis*. Boston: Birkhäuser.

Doupé, D. P., Alcolea, M. P., Roshan, A., Zhang, G., Klein, A. M., Simons, B. D., et al. (2012). A single progenitor population switches behavior to maintain and repair esophageal epithelium. *Science*, *337*, 1091–1093.

Epstein, J. M. (2008). Why model? *Journal of Artificial Societies and Social Simulation*, *11*, 12.

Fletcher, D. A. (2011). To model or not to model? *Molecular Biology of the Cell*, *22*, 909–910.

Foret, L., Dawson, J. E., Villaseñor, R., Collinet, C., Deutsch, A., Brusch, L., et al. (2012). A general theoretical framework to infer endosomal network dynamics from quantitative image analysis. *Current Biology*, *22*, 1381–1390.

French, V., Bryant, P. J., & Bryant, S. V. (1976). Pattern regulation in epimorphic fields. *Science*, *193*, 969–981.

Galliot, B. (2012). Hydra, a fruitful model system for 270 years. *The International Journal of Developmental Biology*, *56*, 411–423.

García-Bellido, A. (2009). The cellular and genetic bases of organ size and shape in Drosophila. *The International Journal of Developmental Biology*, *53*, 1291–1303.

García-Bellido, A. C., & García-Bellido, A. (1998). Cell proliferation in the attainment of constant sizes and shapes: The Entelechia model. *The International Journal of Developmental Biology*, *42*, 353–362.

Gierer, A., Bode, H., Berking, S., Schaller, H., Trenkner, E., Hansmann, G., et al. (1972). Regeneration of hydra from reaggregated cells. *Nature New Biol*, *239*, 98–101.

Gierer, A., & Meinhardt, H. (1972). A theory of biological pattern formation. *Kybernetik*, *12*, 30–39.

Gonsalvez, D. G., Cane, K. N., Landman, K. A., Enomoto, H., Young, H. M., & Anderson, C. R. (2013). Proliferation and cell cycle dynamics in the developing stellate ganglion. *The Journal of Neuroscience*, *33*, 5969–5979.

Goss, R. J. (1969). *Principles of regeneration*. New York: Academic Press.

Gurley, K. A., Rink, J. C., & Sánchez Alvarado, A. (2008). Beta-catenin defines head versus tail identity during planarian regeneration and homeostasis. *Science*, *319*, 323–327.

He, J., Zhang, G., Almeida, A. D., Cayouette, M., Simons, B. D., & Harris, W. A. (2012). How variable clones build an invariant retina. *Neuron*, *75*, 786–798.

Herrera, S. C., Martin, R., & Morata, G. (2013). Tissue homeostasis in the wing disc of drosophila melanogaster: Immediate response to massive damage during development. *PLoS genetics*, *9*, e1003446.

Hobmayer, B., Jenewein, M., Eder, D., Eder, M. K., Glasauer, S., Gufler, S., et al. (2012). Stemness in Hydra—A current perspective. *The International Journal of Developmental Biology*, *56*, 509–517.

Hobmayer, B., Rentzsch, F., Kuhn, K., Happel, C. M., von Laue, C. C., Snyder, P., et al. (2000). Wnt signalling molecules act in axis formation in the diploblastic metazoan hydra. *Nature*, *407*, 186–189.

Hodgkin, A., & Huxley, A. F. (1952). A quantitative description of membrane current and its application to conduction and excitation in nerve. *The Journal of Physiology*, *117*, 500–544.

Höhme, S., Brulport, M., Bauer, A., Bedawy, E., Schormann, W., Hermes, M., et al. (2010). Prediction and validation of cell alignment along microvessels as order principle to restore tissue architecture in liver regeneration. *PNAS*, *107*, 10371–10376.

Höhme, S., Hengstler, J. G., Brulport, M., Schäer, M., Bauer, A., Gebhardt, R., et al. (2007). Mathematical modelling of liver regeneration after intoxication with ccl4. *Chemico-Biological Interactions*, *168*, 74–93.

Howard, J., Grill, S. W., & Bois, J. (2011). Turing's next steps: The mechanochemical basis of morphogenesis. *Nature Reviews Molecular Cell Biology*, *12*, 400–406.
Hufnagel, L., Teleman, A. A., Rouault, H., Cohen, S. M., & Shraiman, B. I. (2007). On the mechanism of wing size determination in fly development. *PNAS*, *104*, 3835–3840.
Ishikawa, H. O., Takeuchi, H., Haltiwanger, R. S., & Irvine, K. D. (2008). Four-jointed is a Golgi kinase that phosphorylates a subset of cadherin domains. *Science*, *321*, 401–404.
Käfer, J., Hayashi, T., Marée, A. F. M., Carthew, R. W., & Graner, F. (2007). Cell adhesion and cortex contractility determine cell patterning in the drosophilaretina. *PNAS*, *104*, 18549–18554.
Kondo, S., & Miura, T. (2010). Reaction–diffusion model as a framework for understanding biological pattern formation. *Science*, *329*, 1616–1620.
Kragl, M., Knapp, D., Nacu, E., Khattak, S., Maden, M., Epperlein, H. H., et al. (2009). Cells keep a memory of their tissue origin during axolotl limb regeneration. *Nature*, *460*, 60–65.
Kücken, M., Soriano, J., Pullarkat, P. A., Ott, A., & Nicola, E. M. (2008). An osmoregulatory basis for shape oscillations in regenerating hydra. *Biophysical Journal*, *95*, 978–985.
Lander, A. D., Gokoffski, K. K., Wan, F. Y., Nie, Q., & Calof, A. L. (2009). Cell lineages and the logic of proliferative control. *PLoS Biology*, *7*, e15.
Lander, A. D., Lo, W. C., Nie, Q., & Wan, F. Y. (2009). The measure of success: Constraints, objectives, and tradeoffs in morphogen-mediated patterning. *Cold Spring Harbor Perspectives in Biology*, *1*, a002022.
Lawrence, P. A., & Struhl, G. (1996). Morphogens, compartments, and pattern: Lessons from drosophila? *Cell*, *85*, 951–961.
Lewis, J. (2008). From signals to patterns: Space, time, and mathematics in developmental biology. *Science*, *322*, 399–403.
Lewis, J., & Wolpert, L. (1976). The principle of non-equivalence in development. *Journal of Theoretical Biology*, *62*, 479–490.
Li, F., Huang, Q., Chen, J., Peng, Y., Roop, D. R., Bedford, J. S., et al. (2010). Apoptotic cells activate the "phoenix rising" pathway to promote wound healing and tissue regeneration. *Science Signaling*, *3*, ra13.
Liu, S.-Y., Selck, C., Friedrich, B., Lutz, R., Vila-Farré, M., Dahl, A., et al. (2013). Reactivating head regrowth in a regeneration-deficient planarian species. *Nature*, *500*, 81–84.
Marciniak-Czochra, A., Stiehl, T., Ho, A. D., Jäger, W., & Wagner, W. (2009). Modeling asymmetric cell division in hematopietic stem cells—Regulation of self-renewal is essential for efficient repopulation. *Stem Cell Dev*, *18*, 377–385.
Martín, F. A., Herrera, S. C., & Morata, G. (2009). Cell competition, growth and size control in the Drosophila wing imaginal disc. *Development*, *136*, 3747–3756.
Meinhardt, H. (1982). *Models of biological pattern formation*. London: Academic Press.
Meinhardt, H. (1983). Cell determination boundaries as organizing regions for secondary embryonic fields. *Developmental Biology*, *96*, 375–385.
Meinhardt, H. (2008). Models of biological pattern formation: From elementary steps to the organization of embryonic axes. *Current Topics in Developmental Biology*, *81*, 1–63.
Meinhardt, H. (2012). Modeling pattern formation in hydra: A route to understanding essential steps in development. *The International Journal of Developmental Biology*, *56*, 447–462.
Merks, R. M. H., Glazier, J. A., Brodsky, S. V., Goligorksy, M. S., & Newman, S. A. (2006). Cell elongation is key to in silico replication of in vitro vasculogenesis and subsequent remodeling. *Developmental Biology*, *289*, 44–54.
Morgan, T. H. (1904). Notes on regeneration. *Biol Bulletin*, *6*, 159–172.
Mori, Y., Jilkine, A., & Edelstein-Keshet, L. (2008). Wave-pinning and cell polarity from a bistable reaction–diffusion system. *Biophysical Journal*, *94*, 3684–3697.

Murawala, P., Tanaka, E. M., & Currie, J. D. (2012). Regeneration: The ultimate example of wound healing. *Seminars in Cell & Developmental Biology*, *23*, 954–962.
Murray, J. D. (2002). *Mathematical biology: I. An introduction* (3rd ed.). New York: Springer.
Murray, J. D. (2003). *Mathematical biology: II. Spatial models and biomedical applications* (3rd ed.). New York: Springer.
Nacu, E., & Tanaka, E. M. (2011). Limb regeneration: A new development? *Annual Review of Cell and Developmental Biology*, *27*, 409–440.
Nakakuki, T., Birtwistle, M. R., Saeki, Y., Yumoto, N., Ide, K., Nagashima, T., et al. (2010). Ligand-Specific c-Fos expression emerges from the spatiotemporal control of ErbB network dynamics. *Cell*, *141*, 884–896.
Nakata, Y., Getto, P., Marciniak-Czochra, A., & Alarcón, T. (2012). Stability analysis of multi-compartment models for cell production systems. *Journal of Biological Dynamics*, *6*, 2–18.
Newman, S. A., Christley, S., Glimm, T., Hentschel, H. G., Kazmierczak, B., Zhang, Y. T., et al. (2008). Multiscale models for vertebrate limb development. *Current Topics in Developmental Biology*, *81*, 311–340.
Nienhaus, U., Aegerter-Wilmsen, T., & Aegerter, C. M. (2009). Determination of mechanical stress distribution in Drosophila wing discs using photoelasticity. *Mechanisms of Development*, *126*, 942–949.
Noble, D. (1962). Modification of hodgkin-huxley equations applicable to purkinje fibre action and pace-maker potentials. *Journal of Physiology-London*, *160*, 317–352.
Noble, D. (2002). Modeling the heart–from genes to cells to the whole organ. *Science*, *295*, 1678–1682.
Nowakowski, R. S., Lewin, S. B., & Miller, M. W. (1989). Bromodeoxyuridine immunohistochemical determination of the lengths of the cell cycle and the DNA-synthetic phase for an anatomically defined population. *Journal of Neurocytology*, *18*, 311–318.
Oates, A. C., Gorfinkiel, N., Gonzalez-Gaitan, M., & Heisenberg, C. P. (2009). Quantitative approaches in developmental biology. *Nature Reviews. Genetics*, *10*, 517–530.
Perez-Garijo, A., Shlevkov, E., & Morata, G. (2009). The role of Dpp and Wg in compensatory proliferation and in the formation of hyperplastic overgrowths caused by apoptotic cells in the Drosophila wing disc. *Development*, *136*, 1169–1177.
Ponti, G., Obernier, K., Guinto, C., Jose, L., Bonfanti, L., & Alvarez-Buylla, A. (2013). Cell cycle and lineage progression of neural progenitors in the ventricular-subventricular zones of adult mice. *PNAS*, *110*, E1045–E1054.
Poss, K. D. (2010). Advances in understanding tissue regenerative capacity and mechanisms in animals. *Nature Reviews. Genetics*, *11*, 710–722.
Reddy, B. V., & Irvine, K. D. (2008). The Fat and Warts signaling pathways: New insights into their regulation, mechanism and conservation. *Development*, *135*, 2827–2838.
Repiso, A., Bergantiños, C., & Serras, F. (2013). Cell fate respecification and cell division orientation drive intercalary regeneration in Drosophila wing discs. *Development*, *140*, 3541–3551.
Rogulja, D., & Irvine, K. D. (2005). Regulation of cell proliferation by a morphogen gradient. *Cell*, *123*, 449–461.
Rogulja, D., Rauskolb, C., & Irvine, K. D. (2008). Morphogen control of wing growth through the Fat signaling pathway. *Developmental Cell*, *15*, 309–321.
Salazar-Ciudad, I., Jernvall, J., & Newman, S. A. (2003). Mechanisms of pattern formation in development and evolution. *Development*, *130*, 2027–2037.
Schier, A. F., & Needleman, D. (2009). Developmental biology: Rise of the source–sink model. *Nature*, *461*, 480–481.
Schröter, C., Ares, S., Morelli, L. G., Isakova, A., Hens, K., Soroldoni, D., et al. (2012). Topology and dynamics of the zebrafish segmentation clock core circuit. *PLoS Biology*, *10*, e1001364.

Schwank, G., Restrepo, S., & Basler, K. (2008). Growth regulation by Dpp: An essential role for Brinker and a non-essential role for graded signaling levels. *Development*, *135*, 4003–4013.

Serrano, N., & O'Farrell, P. H. (1997). Limb morphogenesis: Connections between patterning and growth. *Current Biology*, *7*, R186–R195.

Shimizu, H. (2012). Transplantation analysis of developmental mechanisms in Hydra. *The International Journal of Developmental Biology*, *56*, 463–472.

Shraiman, B. I. (2005). Mechanical feedback as a possible regulator of tissue growth. *PNAS*, *102*, 3318–3323.

Sibly, R. M., Barker, D., Denham, M. C., Hone, J., & Pagel, M. (2005). On the regulation of populations of mammals, birds, fish, and insects. *Science*, *309*, 607–610.

Slack, J. M. W. (1980). A serial threshold theory of regeneration. *Journal of Theoretical Biology*, *82*, 105–140.

Snippert, H. J., van der Flier, L. G., Sato, T., van Es, J. H., van den Born, M., Kroon-Veenboer, C., et al. (2010). Intestinal crypt homeostasis results from neutral competition between symmetrically dividing Lgr5 stem cells. *Cell*, *143*, 134–144.

Staley, B. K., & Irvine, K. D. (2012). Hippo signaling in Drosophila: Recent advances and insights. *Developmental Dynamics*, *241*, 3–15.

Starruß, J., Peruani, F., Jakovljevic, V., Søgaard-Andersen, L., Deutsch, A., & Bär, M. (2012). Pattern-formation mechanisms in motility mutants of Myxococcus xanthus. *Interface Focus*, *2*, 774–785.

Starruß, J., de Back, W., Brusch, L., & Deutsch, A. (2014). Morpheus: A user-friendly modeling and simulation environment for multiscale and multicellular systems biology. *Bioinformatics*, http://dx.doi.org/0.1093/bioinformatics/btt772.

Stocum, D. L. (2012). *Regenerative Biology and Medicine* (2nd ed.). New York: Academic Press.

Tanaka, E. M. (2003). Regeneration: If they can do it, why can't we? *Cell*, *113*, 559–562.

Tanaka, E. M., & Reddien, P. W. (2011). The Cellular Basis for Animal Regeneration. *Developmental Cell*, *21*, 172–185.

Technau, U., Cramer von Laue, C., Rentzsch, F., Luft, S., Hobmayer, B., Bode, H. R., et al. (2000). Parameters of self-organization in Hydra aggregates. *PNAS*, *97*, 12127–12131.

Tomlin, C. J., & Axelrod, J. D. (2007). Biology by numbers: Mathematical modelling in developmental biology. *Nature Reviews. Genetics*, *8*, 331–340.

Trembley, A. (1744). *Mémoires, pour servir à l'histoire d'un genre de polypes d'eau douce, à bras en forme de cornes*. Leiden: Jean et Herman Verbeek.

Turing, A. M. (1952). The Chemical Basis of Morphogenesis. *Philosophical Transactions of the Royal Society of London. Series B, Biological Sciences*, *237*, 37–72.

van der Wath, R. C., Wilson, A., Laurenti, E., Trumpp, A., & Liò, P. (2009). Estimating dormant and active hematopoietic stem cell kinetics through extensive modeling of Bromodeoxyuridine label-retaining cell dynamics. *PLoS ONE*, *4*, e6972.

Wartlick, O., Mumcu, P., Jülicher, F., & Gonzalez-Gaitan, M. (2011). Understanding morphogenetic growth control—Lessons from flies. *Nature Reviews. Molecular Cell Biology*, *12*, 594–604.

Wartlick, O., Mumcu, P., Kicheva, A., Bittig, T., Seum, C., Jülicher, F., et al. (2011). Dynamics of Dpp Signaling and Proliferation Control. *Science*, *331*, 1154–1159.

Wolpert, L. (1969). Positional information and the spatial pattern of cellular differentiation. *Journal of Theoretical Biology*, *25*, 1–47.

Yu, S. R., Burkhardt, M., Nowak, M., Ries, J., Petrásek, Z., Scholpp, S., et al. (2009). Fgf8 morphogen gradient forms by a source-sink mechanism with freely diffusing molecules. *Nature*, *461*, 533–536.